MSc Thesis Mechanical Engineering

Optimization of product handling in the agricultural sector of an underactuated flexure based gripper by using Bayesian estimation

Lorenzo Dominique Nijland

Supervisors: J. J. De Jong, D.M. Brouwer

November 21, 2023

UNIVERSITY OF TWENTE.

Lab of Precision Engineering

Faculty of Engineering Technology

Mechanical Engineering

PREFACE

In front of you lies the master's thesis entitled 'Optimization of product handling in the agricultural sector of an underactuated flexure-based gripper by using Bayesian estimation'. For me this marks the end of my study at the University of Twente. I enjoyed working on the project a lot and I am satisfied with the result that I have achieved with this work.
This work is done for the FlexCRAFT project as part of a continuing research and I hope that my work will add some knowledge to the project and also to the department of precision engineering. I would especially like to thank my supervisor Jan de Jong a lot for his guidance during this project. Our weekly meeting were really helpful and provided insight in the field of grippers. The discussions helped in solving and tackling problems. Furthermore, I want give a word of thanks to Dannis Brouwer for his guidance during my graduation period. I would also like to thank Boi Okken for his feedback and his help with the test setup. Finally, I want to thank my family and friends for all the support during my entire study.

Hengelo, November 2023

CONTENTS

Optimization of product handling in the agricultural sector of an underactuated flexure-based gripper by using Bayesian estimation

L.D. Nijland[1], J.J. de Jong D.M. Brouwer
Department of Precision Engineering - Faculty of Engineering Technology
University of Twente
7500 AE Enschede, The Netherlands
[1]l.d.nijland@student.utwente.nl

Abstract

This research presents a method to optimally estimate the contact forces between an apple and an underactuated flexure-based gripper based on limited sensor information. Based on this estimate a controller maximizes the object acceleration while guaranteeing no-slip and no-crush conditions. Due to cleanability and robustness requirements present in the agricultural sector contact forces cannot directly be measured using force sensors on the gripper fingers, while it is also desirable to limit the number of internal sensors. To find the optimal control parameters an uncertainty parameterization of the apple is presented. In conjunction with a linear force approximation model a Kalman filter is used that allows to estimate the contact forces between the object and the gripper based on sensor information and control input. To find the minimal but still sufficient sensor types and combinations a comparison of single sensors and sensor combinations is made and they are assessed on performance. A test setup is built and used to validate and compare the results of the model and the real situation. In this particular apple usecase an increase in maximal allowable acceleration of about factor 2.4 in horizontal direction and 2.2 in vertical direction was found for an addition of 3 sensors compared to the no sensor approach.

I. Introduction

Nowadays the harvesting of produce still require a large amount of of human labour. But due to many factors such as low wages and health problems this profession is decreasing in popularity [1]. Therefore there is more demand for alternatives to human labour [2]. This raises interest for automation in the agricultural sector.

Studies have shown that there is quite some variety in produce [3] [4] and that this variance is increasing with an increase its overall size [5]. In most of the methods considering the gripping of produce, round (in 2-D) or spherical (3-D) objects are assumed as representations [6]. While this seems like a decent assumption, it will result in less ability to successfully grasp produce with variations. Moreover, variance will result in higher or lower contact forces [7], which could lead to gripping failure or damaging the fruits appearance or pericarp. As a result, research on non-destructive harvesting grippers considering the mentioned requirements is an important topic for harvesting robots [8].

In order to deal with object variance, sensors can be used to measure, and therefore control, contact forces on the contact points. However, in the agricultural environment robustness and hygiene is crucial and the presence of dirt and water is possible [9]. This would require regularly cleaning the gripper and would make the use of force sensors in the phalanges to directly measure the contact forces undesirable. A possibility would be to place sensors else were in the linkage, such that they are not directly in contact with the produce, to provide information on the shape of the produce. This form is sensing is called proprioceptive tactile sensing. [10].

Many different gripper designs are used in the robotic agricultural sector [11]. This research focuses on a underacted gripper. A underactuated gripper has more degrees of freedom (DOF) than the number of actuators, This allows grasping of nonuniform and different sizes of objects [9]. For the joints flexures are frequently used. This is done because, opposed to bearings, flexures require no lubrication thus the gripper is easier to clean, this could benefit hygiene requirements. Moreover, flexures offer no wear and no friction which makes the gripper behave deterministic, which is advantageous for accurate proprioceptive sensing [12].

It has currently not been shown how, and to what extent, this proprioceptive sensing can aid the throughput of agricultural grippers. Therefore this research will introduce a framework that will maximize accelerations acting on the considered produce, introduced by the movement of the gripper, Based on limited sensor information, whilst guaranteeing no-slip and no-crush conditions.

In this paper a parametrization of a selected produce, an apple will be given that captures the variance of the produce. A pseudo-rigid body model (PRBM) of the gripper is introduced and is used for simulations that serve as a base for a bi-linear force approximation model (BLM). This BLM can estimate the contact forces between an object and the gripper based on sensor readings. A method will be presented that uses proprioceptive tactile sensors to estimate object parameters. This method consists of a sensor placement optimization, and a Kalman filter iteration. Improving the acceleration by which the gripper can move an apple will lower the cycle time and improve the performance of pick and place or harvesting processes. To this end a control law will be introduced that finds the optimal actuation force and maximal external force whilst ensuring a successfully grip of the apple. Furthermore, a test setup is built for model validations as well as control law performance verification. A comparison will be made between the simulated model and the performed tests and conclusions will be drawn.

The structure of the paper is partially presented in Figure 1 and is as follows: In section II the methodology of this research is presented, it is divided in several subsections that cover all ingredients that are used in this research. In sections II-C and II-B the usecase for this research will be explained. The design of the gripper is presented and the possible considered sensor types and locations will be listed. Furthermore, a parametrization of an apple is done. In section II-D the non-linear simulation model, on which the method presented in this research is based, is given. Section II-E presents the BLM and all its ingredients that are used to predict the contact forces. Afterwards a control law is presented that optimizes the acceleration in section II-F. The test setup that is built for this research is shown and discussed in section II-H. The results of this research are Presented in section III. Finally in Sections IV and IV a discussion and conclusion of the presented work are given respectively.

II. Methodology

As discussed in the structure of this paper first the usecase will be presented in sections II-C and II-B. In order to present the methodology of this research a subsection is dedicated to the overview of this research in order to get a better understanding of the general flow of the research, this is done in section II-A. Afterwards all parts are explained in detail in their own respective sections and it will be discussed what is expected in the results section.

A. Research overview

Figure 1 introduces an overview of the presented research method. The research flow shows the different models and algorithms, and the order in which they are used in this research accompanied with the dedicated sections. In the first block a parametrization of an apple is generated that is translated to object parameters that are used frequently throughout this research. In the second block the contact forces and sensor readings resulting from these object parameters will be computed by a non-linear simulation, using the PRBM. This block also returns the sensor readings that this object would have given if it was placed in the real test setup. These sensor readings are input for the Kalman block that estimates the object parameters based on sensor readings. The estimated object parameters will be used as input for the contact force approximation to estimate the contact forces. These will be entered into the control law and the optimal control parameters existing of the external force and the actuator force, will be returned. The external force will be related to a maximum allowable acceleration. The dashed box highlights the sections, that together, from the bi-linear force approximation model. The estimated object parameters and contact forces will be compared to the actual values in the results section.

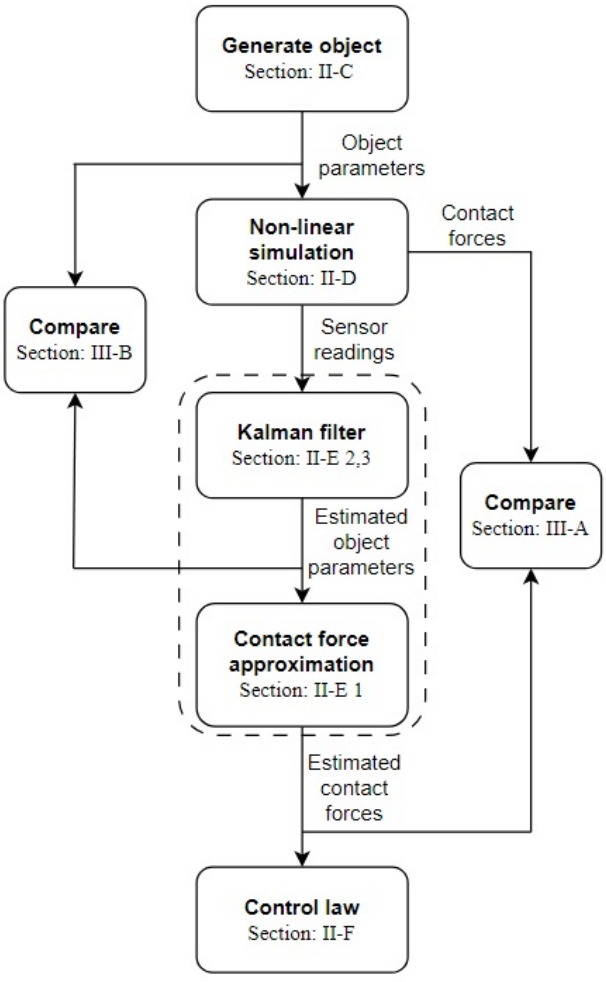

Fig. 1: Research overview presenting the parts of this research accompanied with the relevant sections.

B. Gripper design and sensor placement

The gripper used in this research is based on the work of Dekker et al. [12]. In Figure 2 the design of the gripper is presented. Also the different parts of the gripper are named. The gripper is printed using Nylon PA2200. A parametrization of the gripper including lengths is given in Appendix A. The gripper design is symmetric and has two fingers that are on a 2-D plane. The underactuated gripper kinematically constraints a circular object when all five contact points engage.

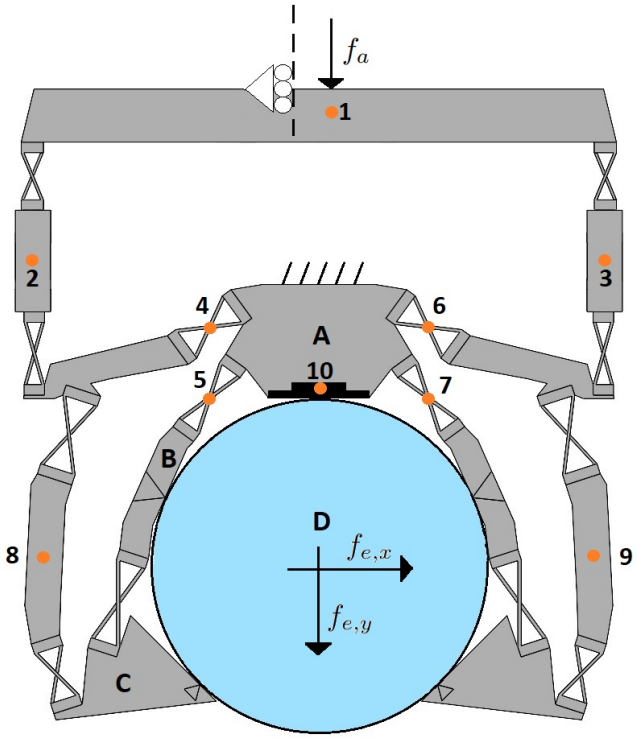

Fig. 2: Gripper design including naming of different bodies, A) fixed middle body, B) left proximal phalanx, C) left distal phalanx D) object. Positioning and numbering of possible sensor candidates. Control inputs actuator force, horizontal and vertical external force.

To estimate the shape of a particular apple that will be picked up, sensors are used. In this research 10 possible sensor candidates are considered. These are also shown in Figure 2. Sensor 1 is a position sensor that measures the vertical distance of which the actuation point is moved. Sensors 2, 3, 8 and 9 are bending beam sensors that measure the force in these members. Sensors 4, 5, 6 and 7 are encoders that measure the angle of these joints. Sensor 10 is a force sensor. This force sensor is now located at the palm. In the real situation this sensor should not be located in the palm due to the earlier mentioned cleanability and robustness requirements. It could, for example, be connected by some sort of link.

C. Object parametrization

As mentioned in the introduction session apples are chosen as produce that will be grasped in this research. Rajokevic et al. [13] processes images of real apples using some polar coordinate system. This allows to show the variance in radius of the apple viewed from above. It is concluded that the radius of acceptable fruit lies between 32.8 and 39.9mm. Whenever the radius lies out of this range the apple is considered deformed. In Figure 3 a example of an acceptable apple and a deformed apple is shown in the polar coordinate system.

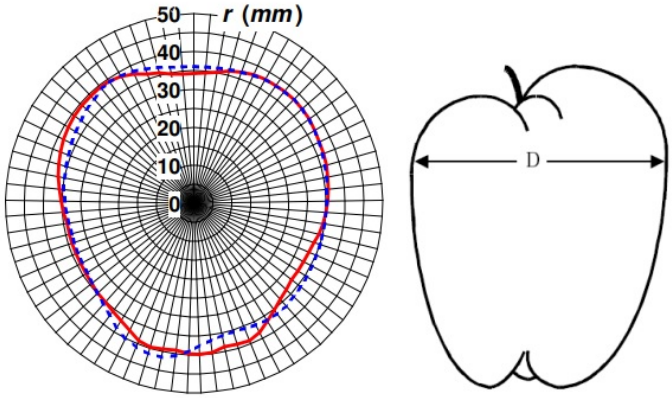

Fig. 3: Left: Radii r (mm) of Red delicious apple fruits of normal shape (solid line) and deformed contour (dashed line) in polar coordinate system. Right: a sketch describing the referent maximal horizontal diameter of apple fruit [13].

Based on this work, variation in position on those five points is introduced. This is shown in Figure 4, Note that this image is not shown in scale for clarity. The centre of the apple is denoted with coordinates x_o and y_o. The other five points have coordinates x_i and y_i such that the vector of object parameters x is:

$$x = (x_o, y_o, x_i, y_i) \qquad \text{for } i = 1, 2, 3, 4, 5. \tag{1}$$

Here i = 1 corresponds with the left proximal phalanx, i = 2 with the left distal phalanx, i = 3 with the right proximal phalanx, i = 4 with the right distal phalanx and i = 5 with the palm. For the rest of this research subscript i corresponds with the same contact points.

The variance of the apples is parameterized by applying a normal distributed variation of the x and y coordinates of these five circles. The shape that is formed by the mean value of all parameters is called the nominal object with nominal object parameters $\bar{x}$. It will be used frequently later on in this research. The standard deviation of all parameters is 1mm. In Figure 5 the shape of a parameterized apple is given in red, whilst the nominal shape is shown in black. In this way the average radius at the contact point is about 38mm which lies in the middle of the acceptable apple range. Apples with radii around these values do typically have a weight of about 150 grams [14]. This value is used later on to determine the maximum allowable acceleration.

According to Chen et al. [8] the maximum force that apples can be grasped with without damaging the pericarp turns out to be $15.35N$. This value is used in this research and will be denoted as f_{bound} being the maximum contact force that does not damage or harm the object.

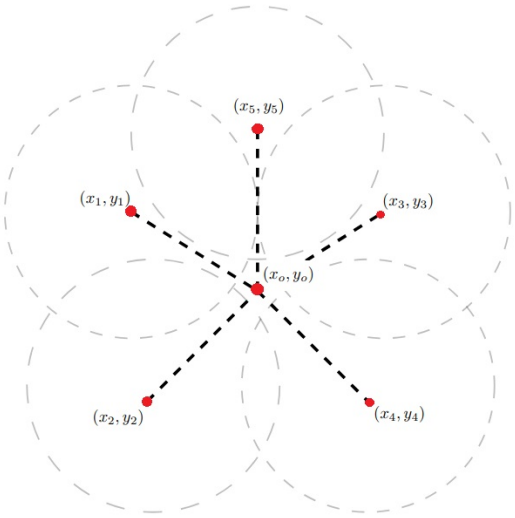

Fig. 4: Parametrization of an apple with introduced coordinates.

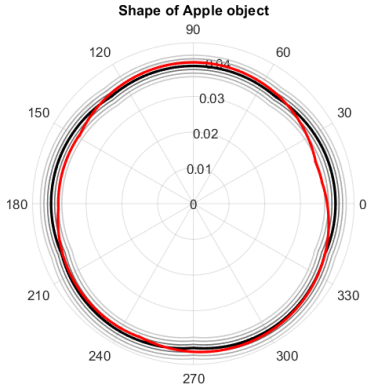

Fig. 5: Nominal apple shape in black, different sigma levels in grey and possible apple shape in red.

D. Pseudo-rigid body model

As mentioned in the introduction SPACAR [15] is used to create a rigid model of the gripper. SPACAR is a flexible multibody dynamics software program that can be used to perform simulations. The model of the gripper consist out of nodes that represent either joints, points on which force is exerted, or contact points. The stiffness of each TFCH is calculated and is added to the joints to resemble the real situation. The nonlinear simulation model returns the contact forces on the object as a function of the shape of the object, the actuation force and the external force. This non-linear simulation model is called the Pseudo-rigid body model and serves as a base to create models in this research. For a more accurate the description of the model see Appendix B.

E. Bi-linear force approximation method

1) Contact force approximation: In order to approximate the contact forces on the object due to the variance in its shape, a force approximation model is created. This model is based on simulations done using the PRBM. The model uses a first order Taylor-approximation around the nominal configuration $\bar{x}$ that yields:

$$f(x,u) \approx \underbrace{f(\bar{x},\bar{u})}_{\bar{f}} + \Delta\hat{f} \tag{2}$$

$$\Delta\hat{f} = (\underbrace{\frac{\partial f}{\partial x}}_{J_f} + \underbrace{\frac{\partial^2 f}{\partial u \partial x}}_{H_f}\Delta u_1)\Delta x + \underbrace{\frac{\partial f}{\partial u}}_{L_f}\Delta u \tag{3}$$

were the vector of contact forces f that follows from the nominal object parameters $\bar{x}$ and applying nominal control parameters $\bar{u}$ is named the vector of nominal contact forces, denoted as $\bar{f}$. Furthermore, $\Delta\hat{f}$ is the term that represents the estimated change in contact forces that depends on $\Delta x = \bar{x} - x$ and $\Delta u = \bar{u} - u$. The Jacobian J_f is a matrix that relates a change in one of the object parameters to a change in contact forces. Since there are 5 contact forces and 12 object parameters J_f is of size 12x5. Furthermore, a change in contact force due to the control parameters is given by matrix L_f (3x5). To get a better understanding of what L_f represents see the visualization shown in Appendix D. Using the PRBM it turns out the external force has a linear relation with the contact forces. The actuation force has a bi-linear effect on the contact forces, to capture this effect the Hessian force H_f is introduced. This bi-linear term captures the effect that a change in object parameters, relative to the nominal parameters, gives a bigger change in contact forces whenever the actuator force is relatively higher.

In order to validate this model contact forces will be computed for a number of sampled objects and these will be compared to contact forces for the same sampled objects following from the PRBM. In this comparison the linear approximation model will also be plotted to highlight the effect of the bi-linear term.

2) Sensor information and sensitivity: The use of the discussed possible sensor candidates offer information about the shape of the object that is being gripped. Here we present linear model that estimates the sensor information based on object parameters:

$$z(x,u) \approx \underbrace{z(\bar{x},\bar{u})}_{\bar{z}} + \Delta\hat{z} + v \tag{4}$$

$$\Delta\hat{z} = (\underbrace{\frac{\partial z}{\partial x}}_{J_z} + \underbrace{\frac{\partial^2 z}{\partial u \partial x}}_{H_z}\Delta u_1)\Delta x + \underbrace{\frac{\partial z}{\partial u}}_{L_z}\Delta u \tag{5}$$

with $\bar{z}$ being the sensor information of a nominal object and v being noise. J_z is the sensor Jacobian that relates a change in object parameters to a change in sensor data. H_z and L_z are the same type of matrices as in the approximation for the contact force. Please note that we here use the notation Δx (without $\wedge$) as the sensor readings are dependent on the true object parameters. In this research the object parameters will be measured whilst applying the nominal control input $\bar{u}$. applying the nominal control input results in Δu being zero. Therefore, the terms H_z and L_z that depend on Δu will be omitted from now on.

3) Kalman filter: In the previous section a linear model is introduced that estimates the sensor information based on object parameters. However, we are interested in an estimation of the object parameters based on sensor information. To do that using equation 4 and 5 the inverse of J_z is needed. But since J_z is not necessarily square or full rank we cannot do this. Previous research dealt with this by using a pseudo-inverse [7] while here we use a probabilistic approach to find an optimal estimate of x. The Kalman filter is a suitable way to estimate the most likely shape that the object has based on sensor readings, considering uncertainties that are present in the form of object variation and noise in sensor readings.

The outcome of the filter is an estimate of the state $\hat{x}$, and the uncertainties that correspond to these states shown in uncertainty matrix P. In order to resemble the real situation the considered noise v is added on top of the sensor values that follow from the non-linear simulation. The first step of the filter is initiation. Then typically 2 steps are repeated. first the filter predicts the states based on a model and then corrects them with measurement data. A Kalman filter generally repeats these steps hence multiple iterations are done. In this research only 1 iteration is used since it is computationally faster and in this way it could be compared to the previous work using the pseudo-inverse. The following terms are used as inputs for the filter:

- Q Process noise uncertainty $[n_{par} \times n_{par}]$
- R Measurement uncertainty $[n_{sen} \times n_{sen}]$
- I Identity matrix

The initiation basically assigns an initial guess of the state and uncertainties to the prior estimates. The initial estimate of the object parameters would be the mean of the object parameters. Furthermore, our initial uncertainty matrix will be a null matrix with the standard deviations of all parameters on the diagonal, for clarity this is denoted as: $P_{est} = \text{diag}(\sigma_i)$. For this particular case the predict step does not affect the prior estimate, being $\bar{x}$, and only adds Q to the prior uncertainty. Therefore these steps are omitted and the values are directly substituted in the following correct step. This is shown in the following three Equations 6, 7 and 8, were in the first equation the Kalman gain K is calculated. This is used to compute the posterior state and its Covariance matrix $\hat{x}$ and P respectively.

$$K = (P_{est} + Q)J_z^T\,(J_z(P_{est} + Q)J_z^T + R)^{-1} \tag{6}$$

$$\hat{x} = \bar{x} - K(\bar{z} - z) \tag{7}$$

$$P = (P_{est} + Q)(I - KJ_z) \tag{8}$$

in which the substitution of $\Delta\hat{x} = \bar{x} - \Delta x$ and $\Delta z = \bar{z} - z$ is applied. $\hat{x}$ is now our estimate of the object parameters and will be input for the bi-linear force approximation model to estimate the contact forces as:

$$\hat{f} = \bar{f} + (J_f + H_f\Delta u_1)\Delta\hat{x} + L_f\Delta u \tag{9}$$

furthermore, the P_n can be related to a uncertainty matrix of the contact forces as:

$$P_f = (J_f + H_f\Delta u_1)P(J_f + H_f\Delta u_1)^T \tag{10}$$

taking the square roots of the diagonal terms yields the standard deviation of the 5 contact forces that will be used in the control algorithm later on. The PRBM is used to sample objects and the sensor values for these objects can be obtained. These sensor values will be used to estimate object parameters using the Kalman filter and will be compared to the actual object parameters in the results section.

F. Optimal contact force control

In the previous subsection the Kalman filter and the bi-linear approximation method have been discussed. Combining these two will provide a estimation of the contact forces in the contact points between the gripper and the object based on sensor readings. Moreover, we also know how the contact forces will be affected by the control parameters by L_f. As mentioned in the introduction the goal of this research is to reduce the cycle time by maximizing the acceleration, and thus the external force, whilst choosing the actuation force such that the object does not slip out and the object is not crushed. By making use of Equation 9, 10 and the following lower and upper bound requirements: $(f_i > 0 \,||\, f_i < f_{bound})$ for i = 1...5, the following conditions are introduced:

$$G_{i,l} : (\hat{f}_i(\hat{x}, [f_e, f_a]) - s\sqrt{P_{f,ii}} > 0) \tag{11}$$

$$G_{i,u} : (\hat{f}_i(\hat{x}, [f_e, f_a]) + s\sqrt{P_{f,ii}} < bound) \tag{12}$$

were the uncertainty matrix P_f is added multiplied with the z-score statistic s. The z-score statistic provides a bound value for which a sample following from this distribution will always remain under for a given percentage. In this research a percentage of 95% is used since exceeding the set bounds will result in a damaged apple, however 100% would decrease the performance too much. In this fashion the contact forces are estimated as function of the estimated object parameters $\hat{x}$, and the control inputs u.

The optimal external forces $f_{e,opt}$ will be solved for a range of chosen actuator forces were each increment is denoted with j. The given equations applies to all 5 contact points which leaves us with 10 solutions for f_e. The lowest of these external force is the maximum allowed external force that does not result in validating any of the set requirements for that increment of actuator force as:

$$f_{e,opt,j} = \min \underset{f_e}{\operatorname{argmax}}(G) \tag{13}$$

were G represent both conditions G_l and G_u. This results in a range of j optimal external forces accompanied with a range of j actuator force increments. The optimal control parameters u_{opt} are determined by finding the highest of these external forces accompanied with the actuator force from that same increment, that is denoted with subscript m, as:

$$u_{opt} = \begin{bmatrix} \max f_{e,opt} \\ f_{a,m} \end{bmatrix} \tag{14}$$

in order to get a better understanding of how this works this principle is visualized in Figure II-F. Note that in this case a 2D-plot is shown but there are actually five dimensions, since there are 5 contact forces. In this Figure an arbitrary object has been sampled and the corresponding contact forces and uncertainties are computed, and are plotted as a point cloud. f_{a2} is the last increment of actuator force that stays inside the box for the given confidence interval and forms, accompanied with the computed external force, the optimal control parameters. for f_{a3} the point cloud lays outside of the box hence, the object would have been crushed.

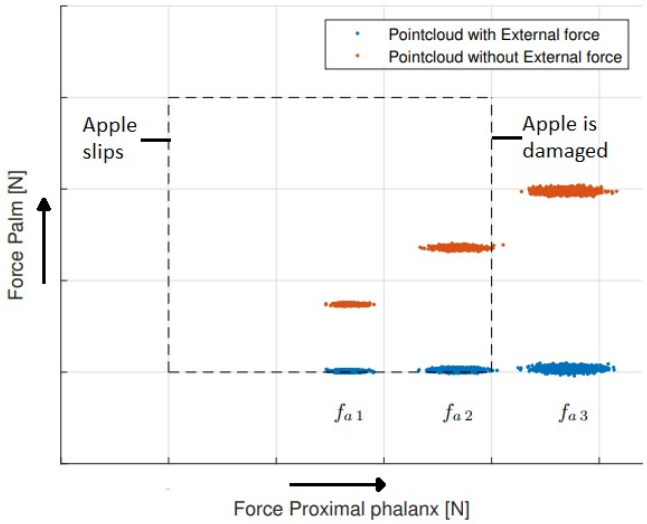

Fig. 6: Principle of the control law visualized. 3 pairs of red (without applied external force) and blue (with applied external force) point clouds are plotted for an increasing actuator force such that $f_{a1} < f_{a2} < f_{a3}$. The dashed box represents the bounds from the set conditions.

In order to assess the performance of the control law the following three cases will be considered:

1) Case 1: A round object without variation that is grasped with no available sensor information.

2) Case 2: A non-round object that is grasped with no available sensor information.

3) Case 3: A non-round object that is grasped with available sensor information.

Case 1 is considered to result in the best performance since for a round object there is no variation thus the contact forces can be determined with no uncertainty, therefore the external force can also be maximized to a maximal value without uncertainties. Case 2 will be the worst case scenario since no sensor information will result in a relatively large uncertainty and therefore maximizing the external force without validating requirements will be minimal. Now Case 3, that represents the real situation, can be assessed on performance by comparison to the other 2 cases. In this case the best sensor combination that is found will be used.

The control parameters and the maximum allowable acceleration will be presented for all three cases in x and y-direction. The maximum allowable external force can be related to the acceleration using the following equation:

$$a = \frac{f_e}{mk} \tag{15}$$

were m is the mass of an apple and k is the safety factor, with a typical factor of 1.2 [16].

G. Optimal sensor strategy selection

As mentioned before 10 possible sensor candidates are considered. The estimation of the object parameters and thus the contact forces depend on what sensor, or sensor combination is used. To assess the performance of the sensors the following quality metrics are considered:

- The error in the estimated parameters due to sensor selection as $e_{mean} = \hat{x} - x$. And the L_2-norm of the error of all object parameters is considered.
- A comparison of how the uncertainty matrix is decreased due to sensor selection. Here the eigenvalues $\lambda_{i\,1,2,..5}$ of P_f are computed.
- The error in the estimated contact forces as $e_f = \hat{f} - f$.
- The optimal control input u_{opt}.

The first performance indicator assesses how good the parameters of an sampled object can be estimated. The second performance indicator shows the uncertainty there is in the the contact forces. This is crucial for the control law since less uncertainty allows to add more actuator and external force that will still result in a successful grasp. Here the eigenvalues are shown instead of the 5x5 uncertainty matrix since they show uncertainty in directions. However, it should be noted that these eigen-directions do not necessarily align with the contact forces. The third performance indicator shows how good the force estimation is. Finally, the fourth performance indicator concludes on what sensor, or sensor combination, allows to maximize the acceleration the most. These quality metrics are first determined for every single sensor to assess the performance. Next combinations of three sensors are made and the quality metrics are applied again to conclude on what combination performs the best.

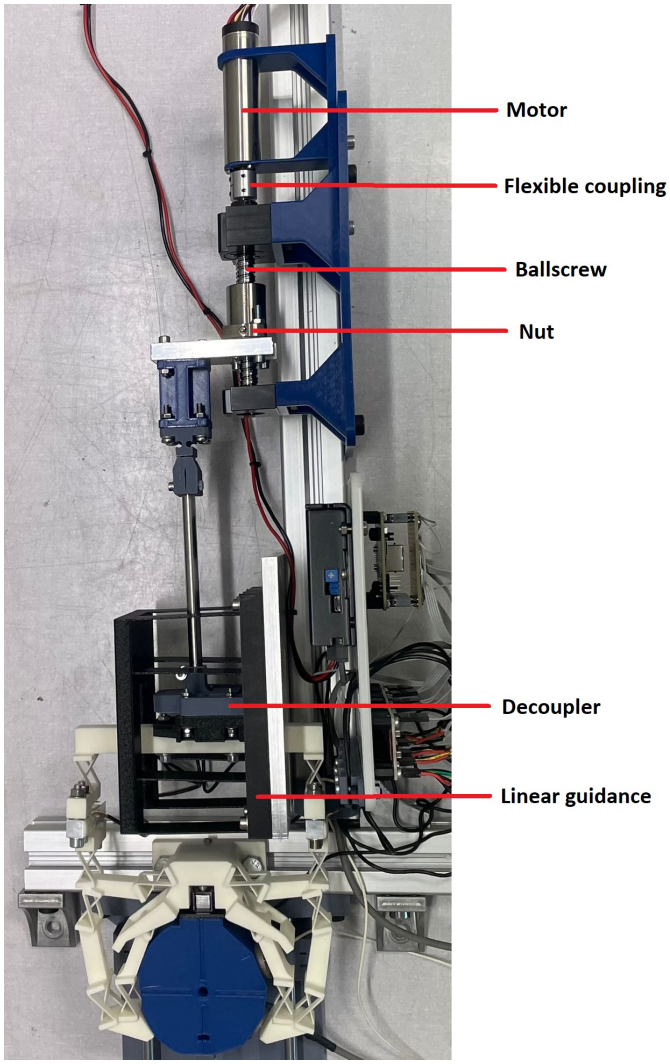

Fig. 7: Test setup with identification of the drive train.

H. Test setup

A test setup is built in order to perform tests and to validate models and values used in this research. In Figure 7 a picture of the test setup is shown. The gripper is actuated by a ECXTQ22XL BL KL A STD 12V Maxon motor. This motor is connected to a R1205K4-FSCDIN-80-1300,023 Hiwin ball-screw. The nut of the ball-screw is connected to a linear guidance and a decoupler.

Via a wire and a pulley a load is connected to the test object this is used to add external forces on the object, in this case the y-direction. Load cells are placed on the inside of the test object such that the contact point makes contact with the gripper. Load cells measure the contact forces on the proximal and the distal phalanx. A bending beam sensor is placed in the palm to measure the contact force (Figure 8), this coincides with sensor candidate number 10. The bending beam sensors are placed on the left and right links of the grippers, they coincide with sensors candidates numbers 2 and 3. Next to being able to measure changes in object size or shape these sensors are also used to determine the actuation force exerted on the gripper as the force passed thought these bending beams together is equal to the actuation force.

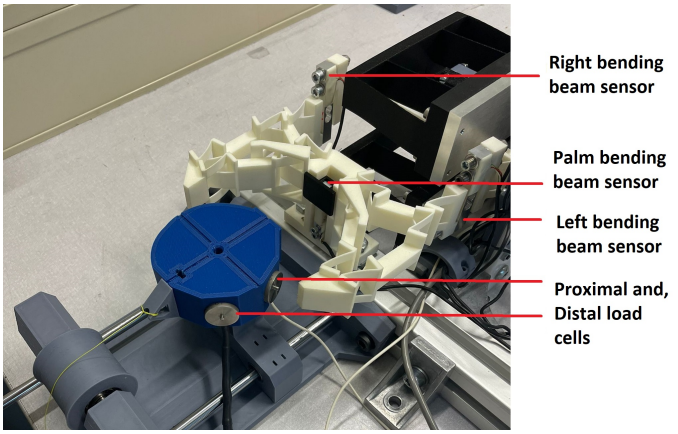

Fig. 8: Used force sensors and their positions.

Using this test setup the following experiments will be conducted.

1) First the Bi-linear force approximation model will be validated by measuring the contact forces for several actuator forces of three parameterized objects. One is the nominal object and the other 2 objects are variations. The shape of the objects is shown in Figure 9, the object parameters can be found in Appendix C. The results are compared to the contact forces following from the non-linear simulations. The contact forces will be measured from 60% to 120% torque with intervals of 10%.

2) The pull-out force estimation is validated by applying an increasing external force, in y-direction, for a given actuator force to see when contact is lost at the palm, and to compare that to the simulated results.

3) Finally the control law will be applied on the same three parameterized objects as in experiment 1. The contact forces that result from applying the found optimal control parameters will be measured and compared to the simulated values.

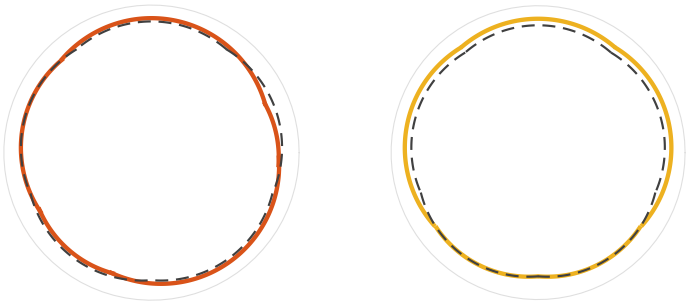

Fig. 9: 2 objects including variations used for testing including nominal shape in dashed black. Variation 1: left, Variation 2: right. Parameters are presented in Appendix C.

Figure 10 shows the sequence of how an object is grasped how the control input is found and applied afterwards. The dashed box represents the bi-linear force approximation once again. Once an object is grasped, it is possible to repeat the sequence that could possibly improve the grasp of the object. The arrow is dotted as, in this research, this possibility is omitted.

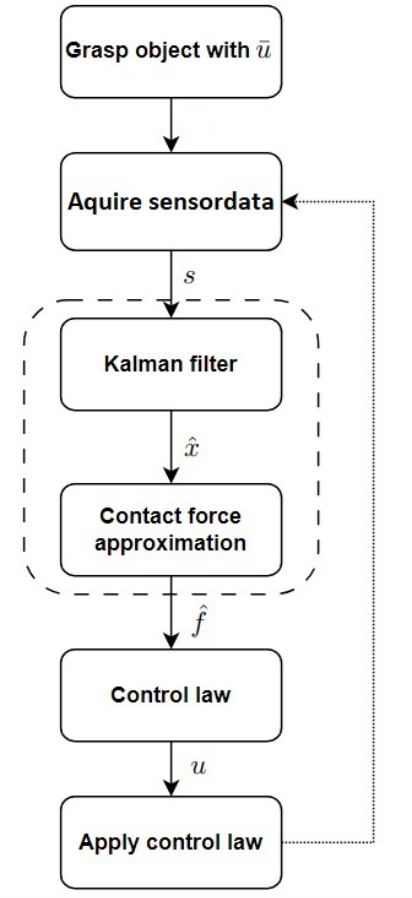

Fig. 10: Sequence of grasping an object and applying optimal control input.

III. Results

A. Bi-linear force approximation model

In Figure 11 the linear and bi-linear force approximation is compared to the non-linear simulation. In the top image the contact force in the left proximal phalanx is presented for 180 different sampled objects. For visualization the sampled variations are sorted from smallest to largest linearly approximated contact force on the left distal phalanx. On the bottom image the error in percentage of both approximations is shown as $e_f = f_{sim}$ - $\hat{f}$ were f_{sim} are the contact forces computed with the nonlinear sim and $\hat{f}$ are the estimated contact forces by linear and bi-linear models. In this plot the first and last 20 samples are removed since the error in those parts increased significantly. The contact forces on the left distal phalanx and the palm for the same 180 samples are presented in Figures 25 and 26 in Appendix D.

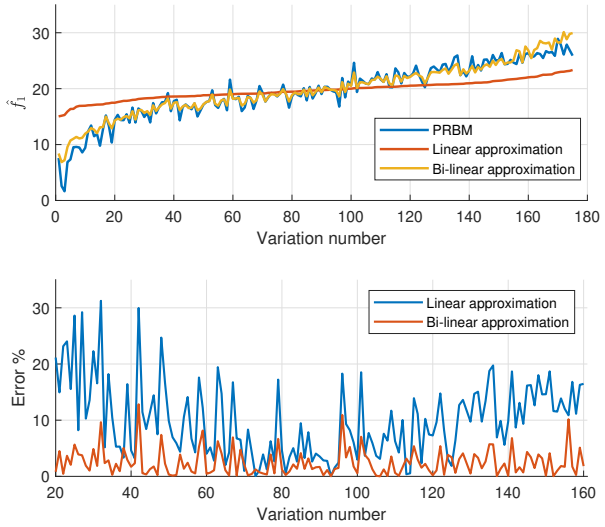

Fig. 11: Top) Comparison of contact force in the left distal phalanx from the linear, bi-linear approximations and the non-linear simulations. Bottom) error of the linear and bi-linear force approximation methods.

It can be observed that the bi-linear force approximation matches the non-linear simulations for the most of the samples. The offset in the first and last 20 samples can be explained by two things. By looking at the last 20 variation numbers for the contact force in the Palm in Figure 26 in Appendix D, it can be seen the contact forces are zero hence there is loss of contact. Contact loss results in a 4-points contact instead of a 5 points contact, and this causes non-linearity. Furthermore, there seems to be a sort of growing offset through the entire curve. In the middle the estimation matches almost fully but at the beginning and in the end the error seems to increase. This is due to the non-linear effect of the parameters of the object on the contact forces. The approximation is only a first order approximation thus, higher order terms are not being captured These effects have higher impact if the object parameters tend to deviate more form the nominal shape which can explain this trend, but due to the normal distributions of all parameters all possible variations do not differ a lot compared to the nominal shape. Overall the error of the bi-linear approximation seems to be less than 5% and therefore the approximation is deemed sufficient.

B. Sensor performance

As mentioned in the methodology section all single sensors and sensor combinations are assessed using quality metrics. Table I shows these quality metrics for a number of single sensors. The full comparison can be found in Appendix E in Table VII.

Sensor	**z**	**0**	**1**	**2**	**8**	**10**
e_x **[mm]**	e_{mean}	2.8	2.7	2.6	2.6	3.0
	e_2	0.8	0.8	0.8	0.8	0.8
P_f **[N]**	λ_1	16.07	16.07	16.07	16.05	2.28
	λ_2	2.28	2.28	1.6e-4	0.11	0.08
	λ_3	0.07	0.07	0.02	0.06	0.04
	λ_4	2.7e-4	2.7e-4	0.07	1.6e-4	2.7e-4
	λ_5	0.02	0.02	0.08	0.01	9.7e-4
e_f **[N]**	$e_{f,1}$	1.23	1.22	1.30	1.27	0.66
	$e_{f,2}$	1.09	1.09	0.78	0.71	1.2
	$e_{f,3}$	1.53	1.53	1.28	1.33	0.67
	$e_{f,4}$	1.42	1.41	0.72	0.79	1.17
	$e_{f,5}$	1.89	1.89	1.89	1.91	0.07
$u_{opt}[N]$	$f_{e,y}$	2.4	2.4	3.3	3.1	4.5
	f_a	36.4	36.4	37.7	38.2	36.7

TABLE I: Performance of selection of single sensors in quality metrics.

The mean and Euclidean norm of the error of the object parameters is similar for all sensors. The estimation of the parameters does also depend heavily on the Kalman filter parameters. In general it can be concluded that sensor 1 alone does not improve anything since the metrics resemble the no sensor situation, denoted with sensor 0. It can be concluded that sensor 10 alone already decreases the uncertainty the most. Sensor 2 and 8 also decrease the eigenvalues of the uncertainty matrix however not the same directions. Sensors 2 and 8 perform similar in the error of the contact forces. It can be observed that sensor 10 relatively decreases the error of contact forces f_1, f_3 and f_5 whilst sensor 2 and 8 decrease the error of contact forces f_2 and f_4. Finally sensor 10 maximizes the external force the most. This sensor directly measures the force at the palm opposed to the sensors that are elsewere in the linkage, which can explain the relatively increase in performance. The performance metrics for the best performing combinations, and the sensor combination present in the test setup, are presented in table II. The table with all considered combinations is shown in Appendix E in Table VIII.

Sensor	z	2,3,10	4,6,10	8,9,10	2,8,10
e_x [mm]	e_{mean}	1.5	4.0	2.7	1.3
	e_2	0.3	1.1	0.8	0.2
P_f [N]	λ_1	0.08	2.28	0.076	0.078
	λ_2	0.07	0.08	0.068	0.074
	λ_3	0.03	0.08	0.00	0.007
	λ_4	1.6e-4	2.7e-4	1.6e-4	1.6e-4
	λ_5	9.7e-4	9.2e-4	6.9e-4	9.2e-4
e_f [N]	$e_{f,1}$	0.19	0.60	0.19	0.21
	$e_{f,2}$	0.27	1.07	0.28	0.28
	$e_{f,3}$	0.18	0.67	0.25	0.16
	$e_{f,4}$	0.30	1.29	0.3	0.47
	$e_{f,5}$	0.08	0.08	0.08	0.08
$u_{opt}[N]$	$f_{e,y}$	4.7	4.9	4.9	5.1
	f_a	36.7	36.5	36.5	36.6

TABLE II: Performance of selection of sensor combinations in quality metrics.

It can be observed that sensor 10 is included in every combination since it performed the best singularly. The smallest error in object parameters is a mean of 1.3mm and a L_2-norm of 0.2mm obtained by sensor combination. 2, 8 and 10. It can be concluded that the sensor combination 8,9,10 decreases the uncertainty in all eigen-directions the most. The smallest error in contact forces is present in either combination 8,9,10 or 2,8,10. Combination 2,8,10 manages to maximize the external force to a value of 5.1 N. This combination exists of the palm sensor 10 in combination with the bending beam sensors 2 and 8. Sensor combination 2,3,10, that is the combination of sensors that is present on the test setup, manages to increase the maximum allowable external force to a value of 4.7 N.

C. Control law simulated

The control law that is described in Section II-F is used on the non-linear simulation model. Table I and II showed that, sensor 10 singularly improves the maximal external force the most. The highest external force can be achieved using sensor combination 2,8,10. The three earlier defined cases are compared and the results are shown in Table III.

Case		1	2	3
u_{opt} horizontal external force	$f_{e,x}$ [N]	17.0	5.0	11.6
	f_a [N]	45.0	31.0	24.3
	a_x [g]	8.0	2.3	5.5
u_{opt} vertical external force	$f_{e,y}$ [N]	9.3	2.4	5.1
	f_a [N]	42.3	40.0	36.6
	a_y [g]	4.4	1.1	2.4

TABLE III: Optimal control parameters of three cases 1) round object, no-variation, no sensor information, 2) non-round including variation, no sensor information, 3) non - round including variation, including sensor information (from combination 2, 8, 10).

The table shows that for the horizontal direction a higher external force can be applied opposed to the vertical direction for all three cases. This is due to how the applied external force is divided over the contact points. In the horizontal case it is divided over both contact points on the left and right phalanx, whilst in the vertical case it only has effect on the palm. This is shown in matrix L_f Appendix C.

It can be concluded that for applying a horizontal acceleration the fully sensorized gripper increases the acceleration to 5.5g from 2.3g for the case were no sensors are applied. This is a factor multiplication of $\approx$ 2.4. for the vertical acceleration this is an increase to 2.4g from 1.1g, which is a factor multiplication of $\approx$ 2.2.

D. Validation of bi-linear force approximation with the test setup

In this section the contact forces estimated by the bi-linear approximation model are compared to the contact forces that are measured from the test setup. The nominal object and two sampled variations are considered. The results are shown in Figures 12, 13 and 14.

For all three objects the measured values match with the simulated values. For the nominal object and variation 2 the proximal contact force is the highest and the palm is the lowest, this is also observed in the experiment. For variation 1 the distal and palm contact force is the highest and the proximal contact force is the lowest. This is also resembles the measured values. It can also be noted that for the simulated results for all three objects the palm only has contact with the object after applying $f_a \approx 15$, $f_a \approx 8$, $f_a \approx 25$ respectively. This is also the reason for the changes in slopes for the same actuator force of the other contact forces.

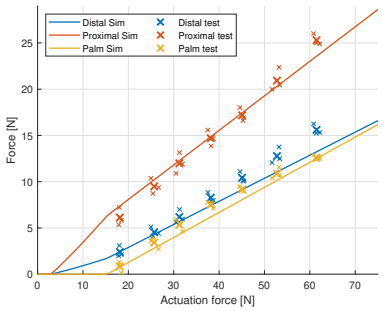

Fig. 12: Comparison of simulated and tested contact forces on nominal object.

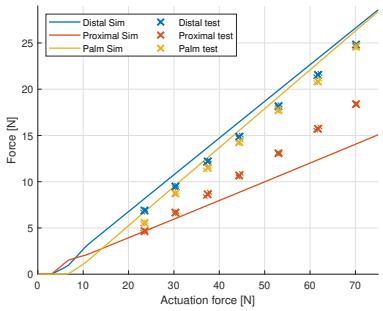

Fig. 13: Comparison of simulated and tested contact forces on Variation 1.

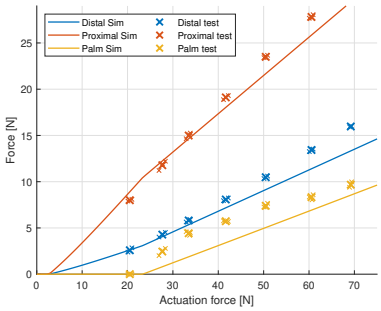

Fig. 14: Comparison of simulated and tested contact forces on Variation 2.

E. Validation of pull-out force curve

In this test the palm contact force is measured to assess, when for a given external force and actuator force, the contact is lost. These measured values are compared to the simulated values, this is shown in Figure 15. The plot shows that there is a difference between the theoretical and actual pull-out force. for an actuation force of 20N this difference is 2N, which linearly increases to about 8N around 47N actuator force. This effect can be explained by the fact that friction is not concluded in the non-linear simulation model. In the real situation, first a certain amount of coulomb friction has to be overcome in order to for the object start moving.

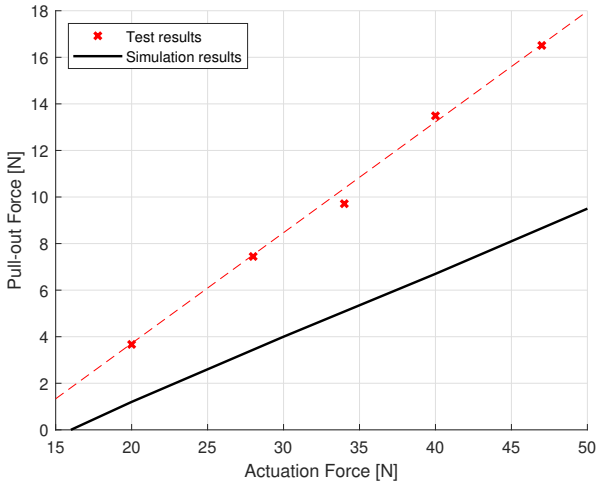

Fig. 15: Comparison of measured pull-out forces (red crosses) and the simulated Pull-out forces (solid black), a linear fit of the measured values is also added (dashed red).

F. Control law used on test setup

In this experiment the performance of the control law applied on the test setup is assessed. In Figure 16 and Table IV the results are plotted and the numerical values are presented respectively. It can be concluded that the generated control inputs on all 3 objects resulted in successful grasps, since the contact forces remain under the bound value. The contact forces for the nominal object and variation 2 are close to the bound of the proximal phalanx. For variation 1 the contact forces are close to the bound of the distal phalanx. This makes sense because reviewing Figures 12, 13 and 14 shows that for the nominal object and variation 2 the contact forces in the proximal phalanx are the highest, whilst for variation 1 the distal phalanx has the highest contact force. All three points measured by the test setup do not really approach the bottom of the plot were the palm contact force is zero. This implies the external force is not fully maximized. The simulated values show that for approximately the same values of external forces the palm contact forces are almost zero. This can be explained by the effect of friction that was also present in the pull-out force experiment.

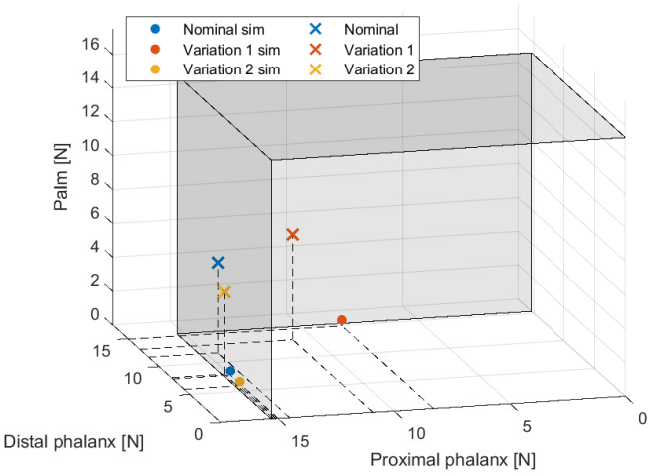

Fig. 16: Control law applied on test setup with the nominal object and two variations, the gray box indicates the maximal and minimal contact force.

	Symbol	Nominal object	Variation 1	Variation 2
u [N]	$f_{e,y}$	5.8 {4.4}	4.9 {5.9}	6.3 {4.3}
	f_a	39 {37}	38 {38}	39 {37}
f_i **[N]**	f_1	14.5 {15.0}	10.9 {8.3}	15.2 {15.1}
	f_2	11.7 {7.8}	13.1 {14.9}	8.0 {5.9}
	f_5	4.3 {0.3}	6.2 {0.4}	3.9 {0.3}

TABLE IV: obtained optimal control parameters and contact forces by applying the control law for the measured values, and simulated values (presented in braces).

IV. Discussion

The simulated and tested results of this research mostly end in successful grasps and for the simulated validations the model match the non-linear simulation. However the results that are obtained by the test setup do not fully resemble the simulated results.

In the model friction between the object and the gripper fingers is not included, this is most likely the main contributor for the difference in simulated an measured results for the pull-out force. In the real situation, an extra amount of coulomb friction has to be overcome in order to pull the object out of the fingers. This difference between the measured results and simulated results is also clearly visible in the results from applying the control law in the simulations and on the test setup.

The gripper is printed out of Nylon PA 2200 which implies creep is present. This effect was also observed whilst doing measurements. The measurements in this research were all taken within approximately 10 seconds after applying control inputs, in this way the effect of creep is minimized.

Due to friction in the system a hysteresis loop is present. This is because of the friction present in the motor, ball screw and straight guidance. This could have affected the measurements if the gripper had to open or close partly. However, the measurements done in this research required the gripper to always open or close fully. In the validation of the bi-linear approximation the same measurements were done multiple times and almost the same contact forces were measured for multiple experiments.

V. Conclusion

This paper delivers a method that maximizes the allowable acceleration applied on an apple that is grasped by a gripper while ensuring no-slip or crushing in face of shape uncertainties. To this end, the shape uncertainties of the apple are estimated using a limited set of sensor in conjunction with a Kalman filter. Based on these estimates the maximal allowable gripper actuator force and robot acceleration are computed that respect bounds on the contact forces.

The presented bi-linear force approximation model manages to give estimations of the contact force within mostly a 5% error compared to the non-linear simulations.

A Kalman filter is used to estimate the most likely object parameters based on sensor information. Using the best performing sensor combination allows to estimate the object parameters with a mean error of 1.3 mm and a L_2-norm of 0.2mm.

A set of different sensors and sensor combination are compared to each other and are assessed on performance. This comparison shows that for single sensors the palm sensor performs the best. By comparing sensor combinations it can be concluded that a combination of the palm sensor and two bending beam sensors can increase the acceleration to 5.5g in the horizontal direction and 2.4g in the vertical direction. These are factors multiplication of 2.4 and 2.2 respectively better compared to the situation were no sensors were available.

A test setup is built and used to validate and compare the results of the non-linear model and the real situation. The measurements validate the bi-linear approximation model and show the effect of friction which is not included in the simulation model.

Based on the results it can be said that this approach for gripping objects is a promising method that can lower the cycle time for handling certain types of produce. It seems this method could also be applied at different types of produce by using the same approach.

REFERENCES

[1] J. F. Elfferich, D. Dodou, and C. D. Santina, "Soft robotic grippers for crop handling or harvesting: A review," *IEEE Access*, vol. 10, pp. 75 428–75 443, 2022.

[2] R. Finger, S. M. Swinton, N. E. Benni, and A. Walter, "Precision farming at the nexus of agricultural production and the environment," *Annual Review of Resource Economics*, vol. 11, no. 1, pp. 313–335, Oct. 2019. [Online]. Available: https://doi.org/10.1146/annurev-resource-100518-093929

[3] Z. Lippman and S. D. Tanksley, "Dissecting the genetic pathway to extreme fruit size in tomato using a cross between the small-fruited wild speciesilycopersicon pimpinellifolium/iandil. esculentum/ivar. giant heirloom," *Genetics*, vol. 158, no. 1, pp. 413–422, May 2001. [Online]. Available: https://doi.org/10.1093/genetics/158.1.413

[4] W. Ji, Z. Qian, B. Xu, W. Tang, J. Li, and D. Zhao, "Grasping damage analysis of apple by end-effector in harvesting robot," *Journal of Food Process Engineering*, vol. 40, no. 6, Jun. 2017. [Online]. Available: https://doi.org/10.1111/jfpe.12589

[5] E. van der Knaap and S. D. Tanksley, "The making of a bell pepper-shaped tomato fruit: identification of loci controlling fruit morphology in yellow stuffer tomato," *Theoretical and Applied Genetics*, vol. 107, no. 1, pp. 139–147, Jun. 2003. [Online]. Available: https://doi.org/10.1007/s00122-003-1224-1

[6] G. A. Kragten and J. L. Herder, "The ability of underactuated hands to grasp and hold objects," *Mechanism and Machine Theory*, vol. 45, no. 3, pp. 408–425, Mar. 2010. [Online]. Available: https://doi.org/10.1016/j.mechmachtheory.2009.10.002

[7] R. Godeschalk, "Quantifying the effect of agricultural product variation on gripping performance, a linear approach," 2022.

[8] K. Chen, T. Li, T. Yan, F. Xie, Q. Feng, Q. Zhu, and C. Zhao, "A soft gripper design for apple harvesting with force feedback and fruit slip detection," *Agriculture*, vol. 12, no. 11, p. 1802, Oct. 2022. [Online]. Available: https://doi.org/10.3390/agriculture12111802

[9] B. Belzile and L. Birglen, "A compliant self-adaptive gripper with proprioceptive haptic feedback," *Autonomous Robots*, vol. 36, no. 1-2, pp. 79–91, Aug. 2013. [Online]. Available: https://doi.org/10.1007/s10514-013-9360-1

[10] ——, "Practical considerations on proprioceptive tactile sensing for underactuated fingers," *Transactions of the Canadian Society for Mechanical Engineering*, vol. 42, no. 1, pp. 71–79, Mar. 2018. [Online]. Available: https://doi.org/10.1139/tcsme-2017-0017

[11] B. Zhang, Y. Xie, J. Zhou, K. Wang, and Z. Zhang, "State-of-the-art robotic grippers, grasping and control strategies, as well as their applications in agricultural robots: A review," *Comput. Electron. Agric.*, vol. 177, no. 105694, p. 105694, Oct. 2020.

[12] J. J. D.M. Brouwer, J.P. Dekker, "Numerical optimization of underactuated flexure-based grippers," 2021.

[13] R. Radojevic, D. Petrovic, V. Pavlovic, Z. Nikolic, and M. Urosevic, "Digital parameterization of apple fruit size, shape and surface spottiness," *African journal of agricultural research*, vol. 6, pp. 3131–3142, 07 2011.

[14] P. Komarnicki, R. Stopa, Ł. Kuta, and D. Szyjewicz, "Determination of apple bruise resistance based on the surface pressure and contact area measurements under impact loads," *Comput. Electron. Agric.*, vol. 142, pp. 155–164, Nov. 2017.

[15] Accessed: 2023-10-18.

[16] Y. Shi, K. Zhu, S. Zhai, D. Zhang, L. Liu, J. Zhao, Y. Long, and Y. Cui, "Design of an apple-picking end effector." *Journal of Mechanical Engineering/Strojniški Vestnik*, vol. 64, no. 4, 2018.

APPENDIX

A. Gripper design

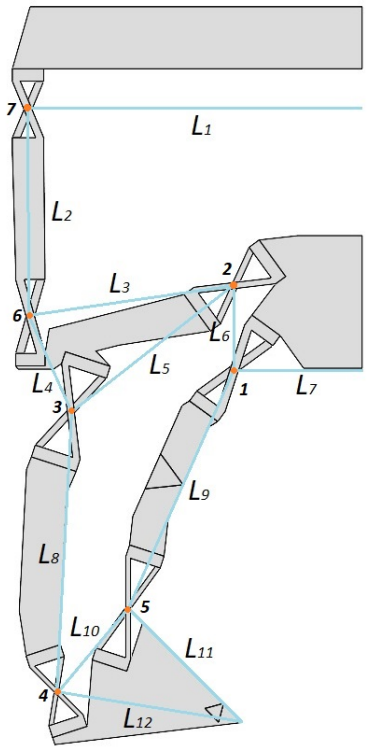

Fig. 17: Gripper design with link lengths.

Symbol	Length [mm]
L_1	68.3
L_2	49.8
L_3	42
L_4	25
L_5	42
L_6	20
L_7	26.3
L_8	54.2
L_9	48.2
L_{10}	15.2
L_{11}	68.3
L_{12}	33.9

TABLE V: Lengths of gripper links.

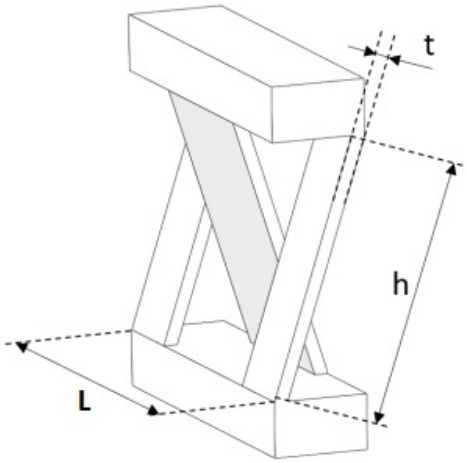

Fig. 18: Parametrization of TFCH.

Hinge	L [mm]	h [mm]	t [mm]	k [n/degree]
1	20	30	0.900	0.130
2	18	33	0.864	0.140
3	22	39	0.790	0.104
4	16	30	0.846	0.135
5	24	33	0.979	0.153
6	18	30	0.799	0.101
7	14	30	0.750	0.107

TABLE VI: Parametrization of TFCH.

B. SPACAR model

In this appendix the SPACAR Model will be explained in more detail. In Figure 19 the model of the gripper is shown. All the blue dots are nodes and the blue lines are elements. All elements are defined by two nodes and conditions are added such as fixing nodes, adding joints or rigidly connecting elements. SPACAR keeps track of all degrees of freedom (DOF) and checks if the system is over or under constraint. In this figure a force is added at the middle top node such that the gripper is actuated and it closes. The red dashed line represents the original configuration. In Figure20 The object is also added. The object exists of a centre node, which is not shown here for clarity, that is rigidly connected to the 5 nodes around it. These 5 nodes are the centres of the circles that define the outline of the object. Again the Circles are not shown here in order to make the Figure more clear.

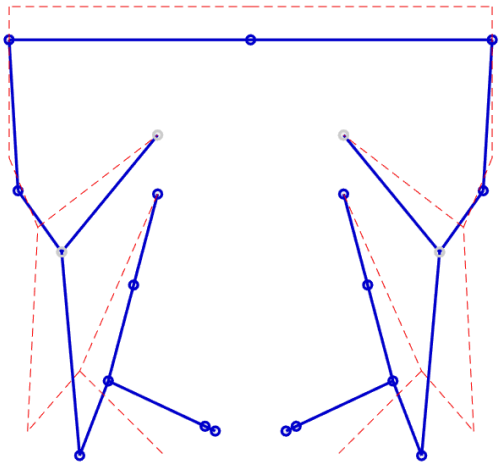

Fig. 19: SPACAR model, dashed lines: original configuration. solid lines: deflected state.

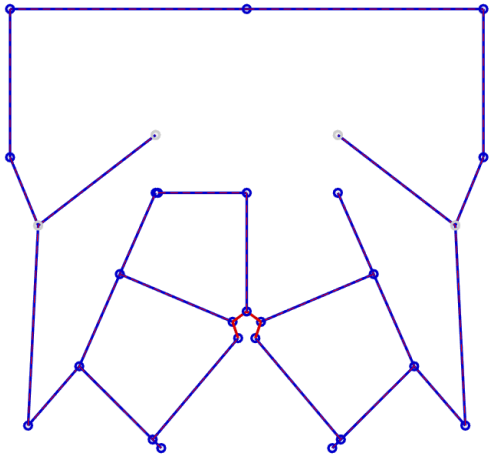

Fig. 20: SPACAR model of gripper with object.

SPACAR does not "Feel" contact between elements. In order to generate contact forces a contact model has to be made. The following contact model has been created. As mentioned before, due to the geometry of the gripper there will be 5 contact points between the gripper and the object. On each of the contact points a perpendicular contact beam is modelled that connects the contact point to the middle of the corresponding circle of the object. Whenever a simulation starts the length of this beam is calculated, this length will then be referred to as L_i. One element is shown in Figure 21 and is denoted with just L. During the simulation the contact point on the beam is free to translate along the phalanx such that the perpendicularity remains. Each of the 5 circles of the object has a radius which in this case is denoted as the threshold length L_{Thr}. Whenever L_0 is smaller than L_{Thr} there is contact and a force applied at the contact point. The contact beam is modelled as a spring and the contact force is thus determined by the amount of displacement, or in the real situation, the amount that the object would be compressed.

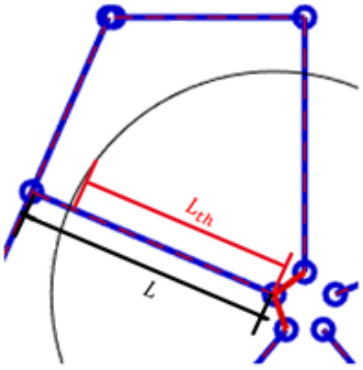

Fig. 21: Visualization of the Contact model, the Length of a contact beam L and the threshold length L_{th}.

C. Nominal values and matrices

$$\bar{x}[mm]^1 = \begin{bmatrix} 0 & -102.0 & -4.8 & 1.5 & -2.9 & -4.0 & 4.8 & 1.5 & 2.9 & -4.0 & 0 & 5.0 \end{bmatrix}$$

$$x_{var1}[mm] \begin{bmatrix} 0 & -102.0 & -4.8 & 1.5 & -2.3 & -3.2 & 3.8 & 1.2 & 3.5 & -4.9 & 0 & 6.0 \end{bmatrix}$$

$$x_{var2}[mm] \begin{bmatrix} 0 & -102.0 & -5.7 & 1.8 & -2.3 & -3.2 & 5.7 & 1.8 & 2.3 & -3.2 & 0 & 6.0 \end{bmatrix}$$

$$\bar{u}[N] = \begin{bmatrix} 0 \\ 0 \\ 20 \end{bmatrix} \qquad \bar{f}(\bar{x}, \bar{u})[N] = \begin{bmatrix} 8.042 & 2.763 & 8.042 & 2.763 & 1.073 \end{bmatrix}$$

$$J_f[N/m] = \begin{bmatrix} -33.1 & 63.2 & 33.1 & -63.2 & 0 \\ 4.1 & -16.7 & 4.1 & -16.7 & -19.0 \\ -937.1 & 614.9 & -640.1 & 50.4 & 1253.9 \\ 403.6 & -222.9 & 271.9 & 56.5 & -386.3 \\ 274.7 & -387.0 & 10.8 & 114.3 & -311.0 \\ 603.6 & -767.3 & 33.4 & 292.3 & -558.0 \\ 640.1 & -50.4 & 937.1 & -614.9 & -1253.9 \\ 271.9 & 56.5 & 403.6 & -222.9 & -386.3 \\ -10.8 & -114.3 & -274.7 & 387.0 & 310.9 \\ 33.4 & 292.3 & 603.6 & -767.3 & -558.0 \\ 0 & 0 & 0 & 0 & 0 \\ -1308.4 & 624.6 & -1308.4 & 624.6 & 1869.8 \end{bmatrix} H_f[N/m] = \begin{bmatrix} -1.5 & 2.7 & 1.5 & -2.7 & 0 \\ 0.26 & 0.71 & 0.26 & 0.71 & 0.43 \\ -40.1 & 27.76 & -25.29 & 2.22 & 54.75 \\ 17.8 & -10.1 & 11.45 & 2.64 & -17.0 \\ 13.69 & -18.27 & 0.36 & 4.61 & -15.13 \\ 26.67 & -27.62 & 1.49 & 11.95 & -18.19 \\ 25.29 & -2.22 & 40.14 & -27.76 & -54.75 \\ 11.45 & 2.64 & 17.8 & -10.1 & -17.0 \\ 0.36 & -4.61 & -13.69 & 18.27 & 15.13 \\ 1.49 & 11.95 & 26.67 & -27.62 & -18.19 \\ 0 & 0 & 0 & 0 & 0 \\ -57.16 & 22.44 & -57.16 & 22.44 & 69.92 \end{bmatrix}$$

$$L_f = \begin{bmatrix} 0.41 & 0.25 & 0.41 & 0.25 & 0 \\ 0 & 0 & 0 & 0 & 0.99 \\ 0.39 & 0.24 & 0.39 & 0.24 & 0.24 \end{bmatrix}$$

$$\bar{s}(\bar{x}, \bar{u}) = \begin{bmatrix} -0.011 & -10.03 & -10.03 & -0.228 & 0.157 & 0.228 & -0.157 & -11.386 & -11.386 & -0.627 \end{bmatrix}$$

$$J_s = \begin{bmatrix} 0 & -46.45 & 46.45 & 0 & 0.81 & 0 & 0.81 & -64.79 & 64.79 & 0 \\ -0.03 & -0.2 & -000 & -0.63 & 0.41 & 0.63 & -0.41 & 5 & 5 & 18.95 \\ -0.38 & -192.46 & 187.24 & -7.99 & 19.26 & 7.99 & -12.47 & -230.25 & 299.75 & -1253.93 \\ 0.09 & 191.98 & -190.67 & 2.0 & -4.82 & -2.0 & 3.12 & 251.31 & -268.71 & 386.34 \\ -0.09 & 166.0 & -167.25 & -1.91 & -2.98 & 1.91 & -2.99 & 251.3 & -213.91 & 310.9 \\ -0.23 & 426.88 & -430.03 & -4.83 & -7.53 & 4.83 & -7.56 & 644.98 & -550.51 & 558.01 \\ 0.38 & -187.24 & 192.46 & 7.99 & -12.47 & -7.99 & 19.26 & -299.75 & 230.25 & 1253.93 \\ 0.09 & -190.67 & 191.98 & 2.0 & -3.12 & -2.0 & 4.82 & -268.71 & 251.31 & 386.34 \\ 0.09 & 167.25 & -166.0 & 1.91 & -2.99 & -1.91 & -2.98 & 213.91 & -251.3 & -310.9 \\ -0.23 & -430.03 & 426.88 & -4.83 & 7.56 & 4.83 & 7.53 & -550.51 & 644.98 & 558.01 \\ 0 & 0 & 0 & 0 & 0 & 0 & 0 & 0 & 0 & 0 \\ 0.24 & 1.64 & 1.64 & 5.03 & 8.32 & -5.03 & -8.32 & -72.07 & -72.07 & -1869.76 \end{bmatrix}$$

[1]The first two elements of any x being (x_o, y_o), describe the position of the center of the object relative to the origin of the SPACAR, in my case the actuation point of the gripper, the other 10 elements describe the positions relative to (x_o, y_o).

D. Linear Force approximation

Below the visualization of the matrix L_f can be seen. L_f exists of vectors that relate change in horizontal- and vertical external force and change in actuator force to changes in contact force. In order to visualize this 3 of the 5 contact forces are chosen such that this can be visualized in a 3D plot (a 5D-plot is not possible). The axis represent the left proximal left, distal and the palm contact forces. The 3 point clouds exist of a number of sampled objects that have been entered in the non-linear simulation to obtain the contact forces. In Figures 22 and 23 the external force components are shown. The different colours represent different applied external forces for a constant actuator force. The arrow points to the direction an increase in external force. In Figure 24 the actuator force component is visualized. Here the external force is kept constant but the actuator force is increased.

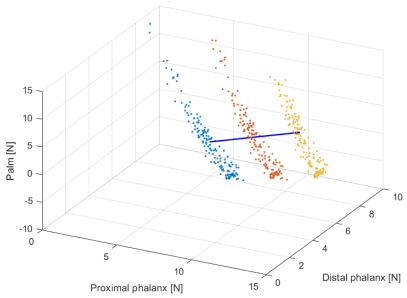

Fig. 22: Visualization of the horizontal component of the external force of the matrix L_f.

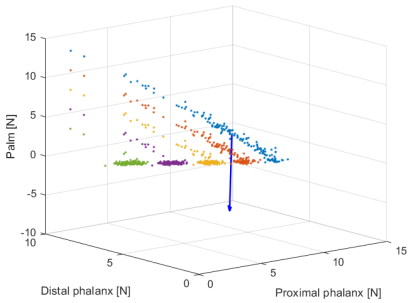

Fig. 23: Visualization of the vertical component of the external force of the matrix L_f.

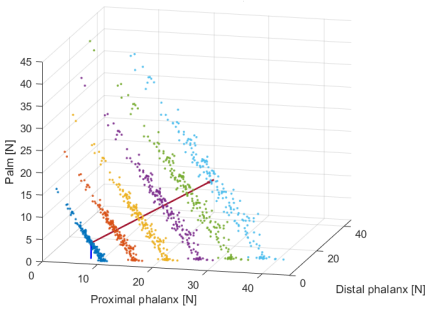

Fig. 24: Visualization of the component of the actuator force of the matrix L_f.

In Figures 25 and 26 the linear and bi-linear force approximations are compared to the non-linear simulation. The contact forces are presented for the same 180 sampled objects. Once again the sampled variations are sorted in the same order as in Figure 11. In the end of Figure 26 it can be seen the contact force determined by the non-linear simulation is zero. This implies there is a loss of contact and this is also the reasons for the offset of the bi-linear approximation at the end of Figures 11 and 26.

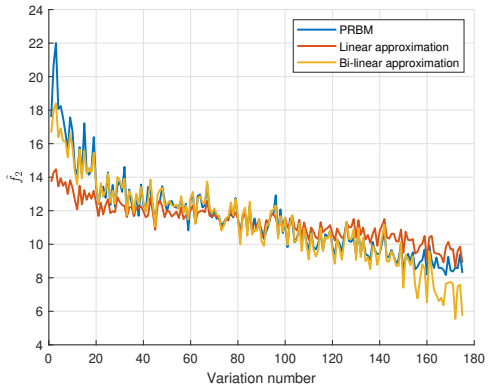

Fig. 25: Validation of the bi-linear force approximation for the Left distal phalanx.

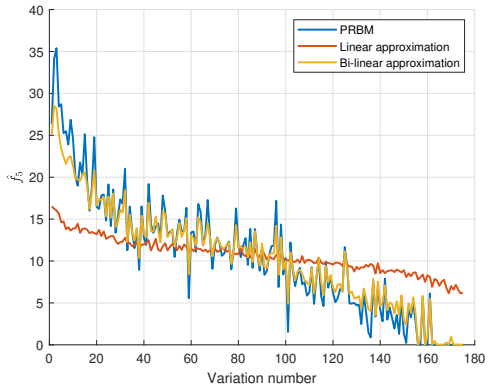

Fig. 26: Validation of the bi-linear force approximation for the palm.

E. Sensor performance

TABLE VII: **Single sensor performance.**

Sensor number	**z**	**0**	**1**	**2**	**3**	**4**	**5**	**6**	**7**	**8**	**9**	**10**
Kalman error [mm]	$\mathbf{e}_{mean}$	2.8	2.7	2.6	2.6	4.1	3.6	4.5	3.6	2.6	2.6	2.99
	$\mathbf{e}_2$	0.82	0.76	0.76	0.76	1.1	0.99	1.2	0.99	0.76	0.76	0.77
Uncertainty [N]	λ_1	16.07	16.07	16.07	16.07	15.91	8.54	16.07	8.54	16.05	16.05	2.28
	λ_2	2.28	2.28	1.6e-4	1.6e-4	2.28	1.39	2.28	1.39	0.11	0.11	0.08
	λ_3	0.07	0.07	0.02	0.02	0.06	0.06	0.07	0.06	0.06	0.06	0.04
	λ_4	2.7e-4	2.7e-4	0.07	0.07	2.7e-4	2.7e-4	2.7e-4	2.7e-4	1.6e-4	1.6e-4	2.7e-4
	λ_5	0.02	0.02	0.08	0.08	0.007	0.008	0.02	0.008	0.01	0.01	9.7e-4
Force error [N]	$\mathbf{e}_{f,1}$	1.23	1.22	1.30	1.30	1.61	3.97	1.27	3.97	1.27	1.27	0.66
	$\mathbf{e}_{f,2}$	1.09	1.09	0.78	0.78	1.08	2.69	0.63	2.69	0.71	0.71	1.2
	$\mathbf{e}_{f,3}$	1.53	1.53	1.28	1.28	1.81	3.12	1.24	3.12	1.33	1.33	0.67
	$\mathbf{e}_{f,4}$	1.42	1.41	0.72	0.72	1.44	1.53	0.56	1.53	0.79	0.79	1.17
	$\mathbf{e}_{f,5}$	1.89	1.89	1.89	1.89	2.35	5.19	1.76	5.19	1.91	1.91	0.07
$\mathbf{u}_{opt}[N]$	$\mathbf{f}_{e,y}$	2.4	2.4	3.3	3.3	2.4	2.8	2.4	2.8	3.1	3.1	4.5
	$\mathbf{f}_a$	36.4	36.4	37.7	37.7	35.9	36.4	35.9	36.4	38.2	38.1	36.7

TABLE VIII: **Sensor combination performance.**

Sensor combination	**z**	**2,3,10**	**4,6,10**	**5,7,10**	**8,9,10**	**2,4,10**	**2,5,10**	**2,8,10**	**4,5,10**	**4,8,10**	**5,8,10**
Kalman error [mm]	$\mathbf{e}_{mean}$	1.5	4.0	4.9	2.7	1.26	1.2	1.26	1.26	1.26	1.26
	$\mathbf{e}_2$	0.27	1.1	1.3	0.79	0.24	0.22	0.24	0.24	0.24	0.24
Uncertainty [N]	λ_1	0.08	2.28	0.58	0.076	0.076	0.076	0.078	2.28	0.808	0.808
	λ_2	0.07	0.08	0.08	0.068	0.077	0.077	0.074	0.76	0.074	0.074
	λ_3	0.03	0.08	0.01	0.00	0.01	0.01	0.007	0.008	0.011	0.011
	λ_4	1.6e-4	2.7e-4	2.6e-4	1.6e-4	1.6e-4	1.6e-4	1.6e-4	2.7e-4	1.63e-4	1.63e-4
	λ_5	9.7e-4	9.2e-4	9.2e-4	6.9e-4	9.5e-4	9.5e-4	9.2e-4	9.2e-4	9.44e-3	9.44e-3
Force error [N]	$\mathbf{e}_{f,1}$	0.19	0.60	1.79	0.19	0.22	0.22	0.21	0.53	0.34	0.28
	$\mathbf{e}_{f,2}$	0.27	1.07	3.34	0.28	0.61	0.62	0.28	0.96	0.25	0.29
	$\mathbf{e}_{f,3}$	0.18	0.67	1.86	0.25	0.20	0.20	0.16	0.5	0.22	0.23
	$\mathbf{e}_{f,4}$	0.30	1.29	3.45	0.3	0.62	0.54	0.47	1.05	0.98	0.86
	$\mathbf{e}_{f,5}$	0.08	0.08	0.08	0.08	0.08	0.08	0.08	0.08	0.08	0.08
$\mathbf{u}_{opt}[N]$	$\mathbf{f}_{e,y}$	4.7	4.9	4.4	4.9	4.8	4.7	5.1	4.9	4.8	4.6
	$\mathbf{f}_a$	36.7	36.5	35.6	36.5	36.2	36.4	36.6	36.5	36.2	36.8